ELSEVIER

S1359-835X(96)00053-X

Composites Part A **27A** (1996) 821–832

1359-835X/96/$15.00

Elasto-plastic finite element modelling of interfacial failure in model Kevlar 49 fibre–epoxy composites

R. B. Nath and D. N. Fenner
Department of Mechanical Engineering, King's College London, Strand, London WC2R 2LS, UK

and C. Galiotis*
Department of Materials, Queen Mary & Westfield College, Mile End Road, London E1 4NS, UK

Elasto-plastic finite element analysis has been used to model a single unsized Kevlar 49 fibre embedded in an epoxy matrix subjected to tensile loading. The predicted axial stress distribution along the fibre is compared with experimental data, obtained using the technique of laser Raman spectroscopy, for a number of incremental applied strain levels. The geometry of the fibre end has been modelled employing an analytical fibre end fibrillation model (FEFM). Furthermore, the influence of residual stresses in the system due to curing, has been analysed. Good correlation is obtained with the experimental data and it is shown that the mode of interfacial failure in the composite involves yielding at the fibre–matrix interface initiating at the fibre end.

(Keywords: finite element; elasto-plastic; fibrillation; fibre end; laser Raman spectroscopy; Kevlar 49; epoxy resin)

INTRODUCTION

When a fibre reinforced composite is loaded, most of the load is transferred via the matrix to the fibre. Due to the difference in the elastic moduli of the fibre and matrix, interfacial shear stresses (ISS) are induced at the fibre–matrix interface. Theoretical predictions of the ISS distribution along the interface have been made by several authors, notably Cox[1], for the case where both matrix and fibre are assumed to be linear elastic and the fibre–matrix interface remains intact. In reality, however, as the tensile loading on the specimen increases, the shear stress at the interface reaches a critical value, termed the interfacial shear strength (IFSS) for the system. Beyond this point one or more modes of interfacial failure are observed experimentally[2–9]:

- *Mode* α. Matrix yielding at the intact interface. This mode has already been observed to occur in Kevlar fibre–epoxy matrix systems[2,4].
- *Mode* β. A crack initiates at the fibre end and propagates along the interface. Frictional stress transfer between the fibre and matrix may take place across the crack faces. This failure mode has been observed to occur in glass fibre systems[10,11].
- *Mode* γ. A conical crack initiates at the fibre end and propagates into the matrix at an angle to the axis of the fibre[10,12].

The axial stress distribution along the fibre has been measured experimentally for crystalline fibre–matrix systems using the technique of laser Raman spectroscopy (LRS)[2–9]. This technique relies on the fact that the Raman frequency of the atomic vibrations of crystalline reinforcing fibres, such as aramid or carbon, depends on the axial component of stress, σ_f, in the fibre[2]. Unique Raman frequency *versus* σ_f calibration curves, produced for each type of fibre, are used to convert the measured Raman frequency variation along an embedded fibre to an axial stress distribution.

For the unsized high modulus carbon fibre–epoxy matrix system, the axial stress distribution becomes S-shaped towards the fibre ends as the applied strain is increased[9]. The ISS is zero at the fibre ends and has a

* To whom correspondence should be addressed

take-up region followed by the normal elastic profile. It has been found in a previous work, that Mode γ interfacial failure is consistent with the experimental data, for this carbon–epoxy composite system[13,14].

For discontinuous Kevlar 49 fibre–epoxy composites[2,4,6], the axial stress distribution after interfacial failure is trapezoidal in shape. The maximum ISS is constant at a value of approximately 45 MPa near the fibre ends and then decays to zero away from the fibre ends, in a Cox type elastic manner. The value of 45 MPa is the shear yield stress of the bulk matrix, so support is given to the micrographic evidence which indicates that interfacial plastic deformation occurs as the applied strain on the composite is increased[2]. This suggests a Mode α interfacial failure for the Kevlar 49–epoxy composite system.

Guild *et al.*[4] have modelled a Kevlar 49 short fibre embedded in an elasto-plastic epoxy matrix, using finite element (FE) analysis. Fair correlation between FE and experimental fibre stress data was achieved, but exceptionally high von Mises interfacial strains were predicted at the fibre end. These von Mises matrix strains were found to be much higher than is physically reasonable in a real composite specimen. For example, for an applied strain of 1.2%, a von Mises strain of 60% was predicted. This was found to occur for both a rounded fibre end and a sharp corner, indicating that the sharp corner was not the cause of the von Mises strain concentration.

The reason for such a strain concentration was that account had not been taken of the real nature of the fibre end geometry, as shown in Figure 1 of Guild *et al.*[4]. When a Kevlar fibre is cut using ceramic scissors, the end is not cleanly cut, as is the case with a carbon fibre, but is splayed out (*Figure 1*). The cutting process itself applies greatest shear stresses to the surface layers of the fibre, which in the case of Kevlar, causes extensive fibrillation fo the fibre end. This *fibrillated zone* consists of numerous Kevlar fibrils interspersed with matrix. In this zone, the effective radius of the fibre is increased whilst there is a corresponding dilution of the material properties of the fibre by those of the matrix (*Figure 2*).

To account for this complex fibre–matrix interaction, two analytical models are presented in which the material properties are inhomogeneous. They are a one-dimensional model, in which the material properties of the fibrillated zone are considered to vary with axial coordinate, z, and a two-dimensional model, where the variation is both a function of axial and radial, r, coordinates.

FE ANALYSIS OF COMPOSITES

The results obtained from an FE analysis of a composite specimen, must satisfy certain criteria. These criteria are based on the upper bounds on the values of stress or strain, at any point in the specimen model, defined by the real material behaviour:

I—At any point in the fibre, the von Mises equivalent stress must be lower than the fracture stress of the fibre, σ_f^*:

$$\sigma_f < \sigma_f^*$$

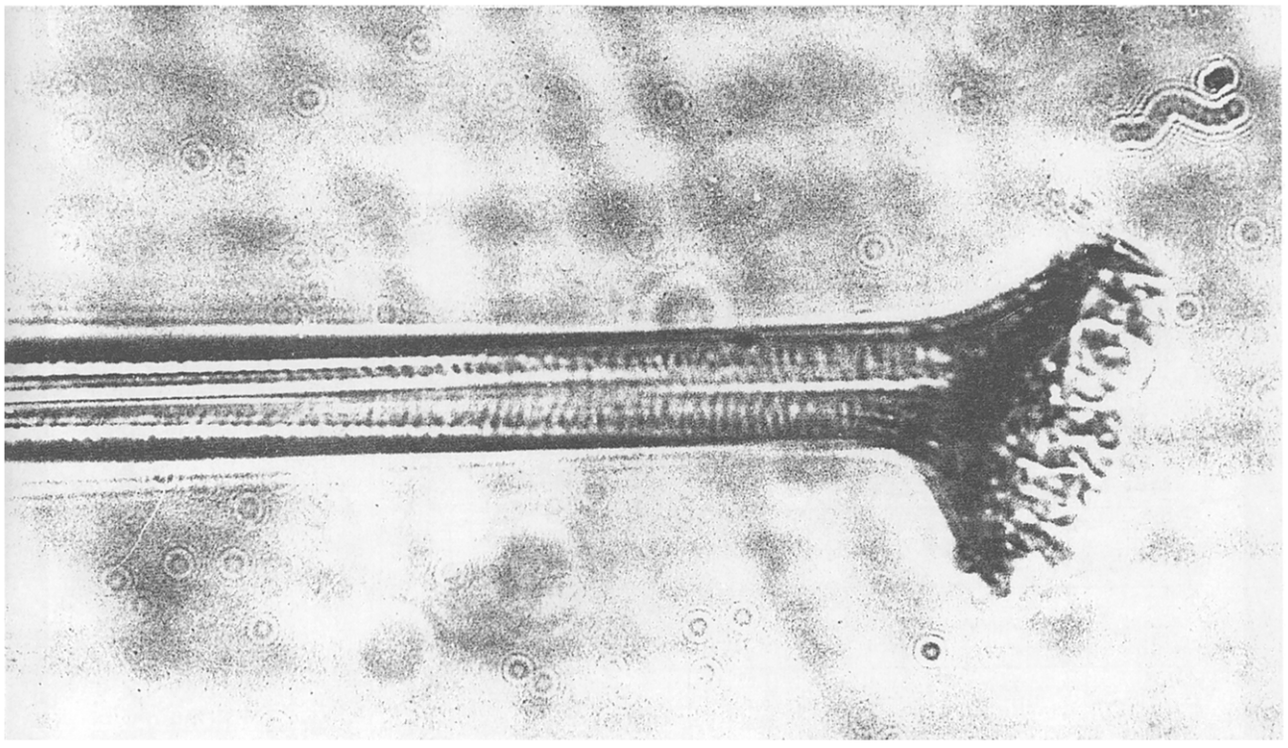

Figure 1 A typical fibrillated Kevlar 49 fibre end cut by razor/ceramic scissors. The diameter of the fibre is 12 μm

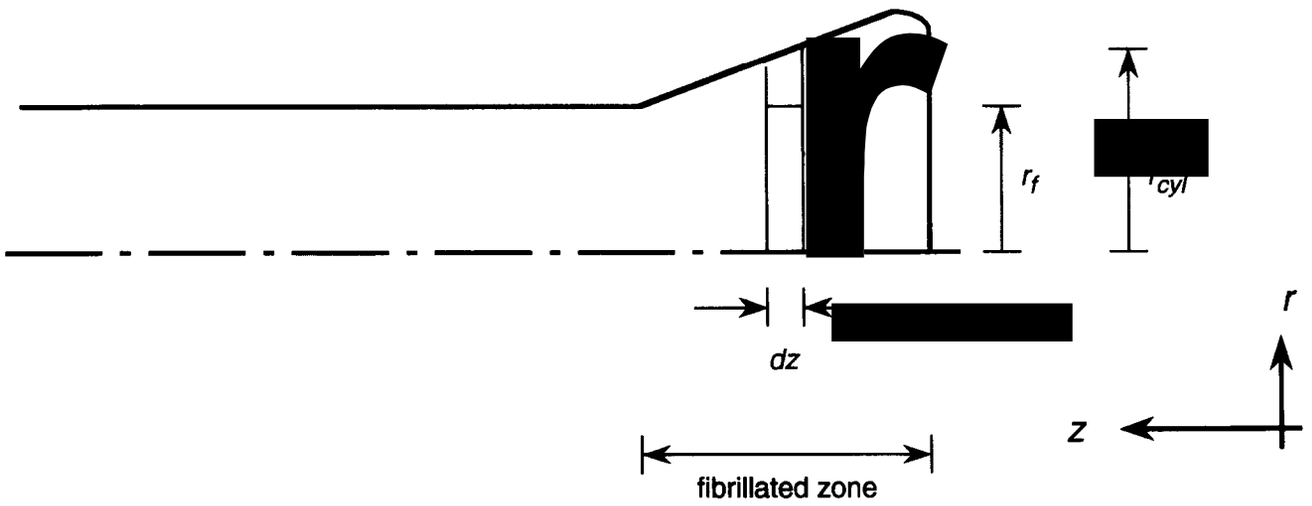

Figure 2 Geometry of fibrillated fibre end

II—At any point in the matrix, the von Mises equivalent stress must be lower than the *relaxed* tensile yield stress of the matrix, σ_m^{yield}, for the given applied strain rate:

$$\sigma_m < \sigma_m^{yield}$$

III—At any point in the matrix, the von Mises equivalent strain must be lower than the tensile fracture strain of the matrix, ϵ_m^*:

$$\epsilon_m < \epsilon_m^*$$

Element geometries must satisfy the various mesh element quality tests, as regards element corner angles and aspect ratios[15]. Care must be taken to ensure that the mesh is sufficiently refined in areas of high stress/strain gradients, i.e. the *discretization error* must be minimal. This may be achieved through the use of mesh refinement[15], especially in areas of high stress or strain gradients.

The values of the various criteria limits, for the Kevlar–epoxy system, are $\sigma_f^* = 3.6$ GPa, $\sigma_m^{yield} = 31$ MPa and $\epsilon_m^* = 4.2$, for the given strain rate. In a number of cases[16–23], criteria II and III are violated. This is invariably due to the fact that the matrix is assumed to behave in a linear-elastic manner. In addition, some of the meshes fail the FE based criteria, thus predicting erroneous stress states[16,19].

EXPERIMENTAL MEASUREMENTS

The model composite tested comprised a single Kevlar fibre embedded in an epoxy resin. The fibres, supplied by Du Pont, were approximately 12 μm in diameter and a Ciba-Geigy LY5052/LY1927 epoxy resin was used. Full details of the manufacturing procedure are given in ref. 4.

The composite was subjected to incremental tensile loading. Using the technique of LRS, the axial stress distribution along the length of the fibre was obtained for various values of the applied strain, e_{app}. Values of axial stress in the fibre were taken for each point along the fibre, by averaging the experimental data at both ends of the fibre.

Raman spectra were obtained using the 514.5 nm (green) line of an Ar-ion laser as the excitation wavelength. The laser beam was directed through a series of mirrors to a modified Nikon microscope which was used to focus the laser beam to a 2 μm spot on the fibre via a suitable objective lens. The 180° backscattered beam was collected by the same microscope objective and focused on the entrance slit of a SPEX 1877 triple monochromator spectrometer. In order to reduce the effective scattering volume to the region of the depth of focus in the fibre, the scattered beam was focused onto a 200 μm pinhole before it entered the spectrometer. Finally, the spectrometer dispersed light was directed to Wright Instruments CCD (charge coupled device) detector, employed as the photon detecting system, and the Raman spectrum was recorded on a PC for specific wavelength windows. All frequency peak values have been derived by applying Lorentzian fitting routines to the raw data obtained by the CCD detector.

FINITE ELEMENT ANALYSIS

The axisymmetric FE model of the composite specimen (*Figure 3a*) covers one quarter of the diametral section, due to the symmetry of the problem (*Figure 3b*). The length of the fibre considered was 480 μm, which is substantially greater than the transfer length of the system. The mesh consisted of three-noded triangular and four-noded quadrilateral axisymmetric linear elements. The loading took the form of a uniform displacement imposed on those nodal points lying on the end face of the composite. The FE meshes were generated using FEMGEN/FEMVIEW and the solutions were obtained using ABAQUS 5.2.

In order to include the residual stresses in the composite induced thermally during curing, it is

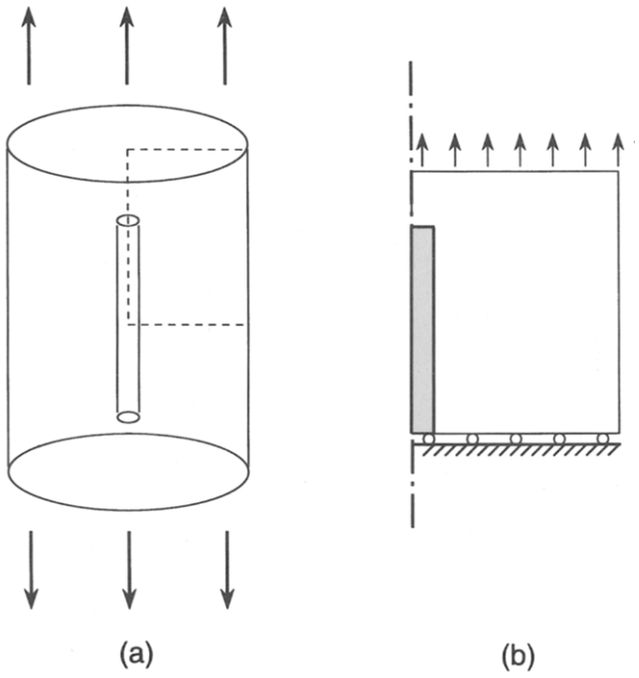

Figure 3 (a) Composite specimen; (b) FE model geometry

necessary to understand the method of fabrication. Matrix resin is heated to approximately 90°C and the correct amount of curing agent or hardener is then added. The material is then poured into a mould and after about 15 min, a fibre is then laid onto the surface of the now viscous matrix. The fabrication is then completed by adding another layer of matrix. On cooling of the composite specimen, a *gelation* occurs in the matrix, whereupon it goes from being a viscous fluid to a solid. The temperature at which this gelation occurs is estimated to be 70°C.

To model this process, a uniform temperature drop of 50°C was applied to all nodes in the FE model. The mechanical loading was subsequently applied to the model as described below. The thermal expansion coefficient differential that exists between the fibre and matrix (see *Table 1*) induced stresses in both the fibre and locally in the interfacial region of the matrix.

The material properties for both fibre and matrix are given in *Table 1*. The matrix is assumed to exhibit perfect plasticity after a von Mises equivalent strain of 4.2% has been reached. The corresponding tensile yield stress at this value of strain was 78 MPa. The matrix was modelled as isotropic and the fibre was assumed to be elastic and transversely isotropic.

Since polymers exhibit substantial *viscoelasto-plastic* behaviour, the *relaxed* stress–strain behaviour must also be considered. The matrix, over the duration of the experiment, undergoes a certain amount of stress relaxation, thus reducing by a certain factor its effective elastic modulus. This factor has been found to be 0.6, at room temperature, and thus, the final *relaxed* tensile yield stress was calculated to be 31 MPa[2].

An initial confirmation of the plain fibre end, as

Table 1. Material properties

	Kevlar 49 fibre	LY5052/1927 matrix (relaxed)
Axial tensile modulus	115 GPa	1.78 GPa
Transverse modulus	7 GPa	1.78 GPa
Axial tensile strength	3.6 GPa (fracture)	31 MPa (yield)
Axial fracture strain	2.9%	4.2%
Axial Poisson's ratio	0.40	0.36
Transverse Poisson's ratio	0.33	0.36
Axial CTE[a]	-5.2×10^{-6} (K^{-1})	58×10^{-6} (K^{-1})
Transverse CTE[a]	41.4×10^{-6} (K^{-1})	58×10^{-6} (K^{-1})

[a] Coefficient of thermal expansion

modelled by Guild *et al.*[4], was made. The fibre was modelled with a rounded end, as shown in *Figure 4*.

A four finite-size cylinder approximation was made of the fibrillated zone according to the 1-D FEFM (fibre end fibrillation model) (see equations (A1), Appendix). Each cylinder was assigned elastic moduli calculated using a mean r_{cyl} for the respective cylinder. A five by four discretization of the fibrillated zone was then modelled, according to the 2-D FEFM (see equations (A2), Appendix). Thus each of the four cylinders, used in the 1-D FEFM model, was subdivided into five concentric rings. The assignment of elastic moduli to each ring was then based on mean values of radial distance of the respective ring. All cylinders and rings were modelled as transversely isotropic, in line with the assumptions of the FEFM. The levels of applied strain that were applied experimentally and used to match the FE data to, were 0.5, 0.7, 1.0 and 1.3%.

RESULTS AND DISCUSSION

Simple fibre end model

The undeformed mesh, in the region of the fibre end, is shown in *Figure 4*. The von Mises strain concentration which occurs at the fibre corner ($z = 0$), is 200%, for e_{app} of 1.0%, as shown by the von Mises strain distribution along the fibre (*Figure 5*). The reason for the substantial increase in this value, in comparison with Guild *et al.*'s[4] result of 30%, for the same model, is possibly due to the higher degree of mesh refinement in this area of high strain gradients. A typical mesh element size in this region was 2 μm in the Guild model, whereas it is 0.4 μm in the present analysis. This result confirms the inadequacy of the simple fibre end model in predicting the state of stress and strain in the real fibre composite, subjected to tensile loading.

Due to this high von Mises strain concentration, a violation of criterion III has occurred, thus invalidating these FE stress and strain fields as being a solution to the interfacial failure problem, for the Kevlar–epoxy system.

1-D FEFM

The undeformed and deformed FE meshes in the

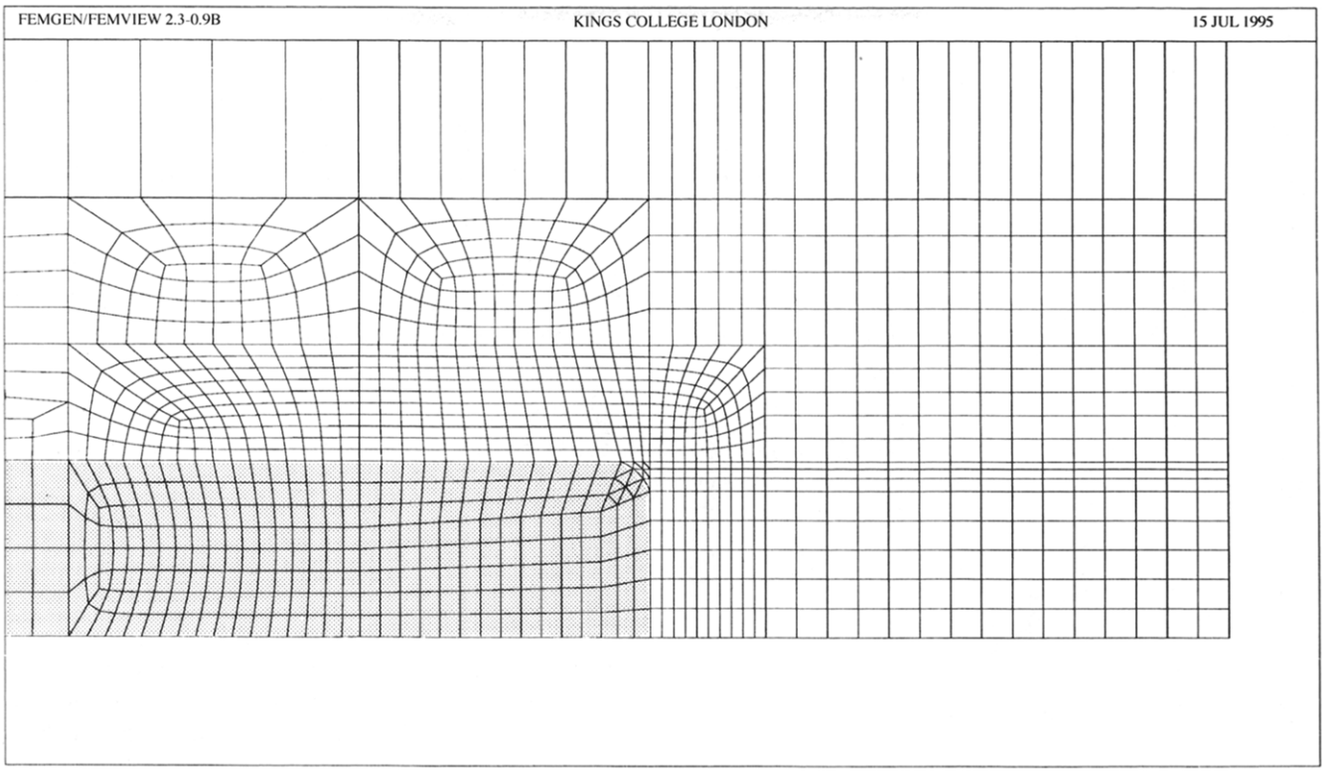

Figure 4 Simple fibre end model: undeformed mesh

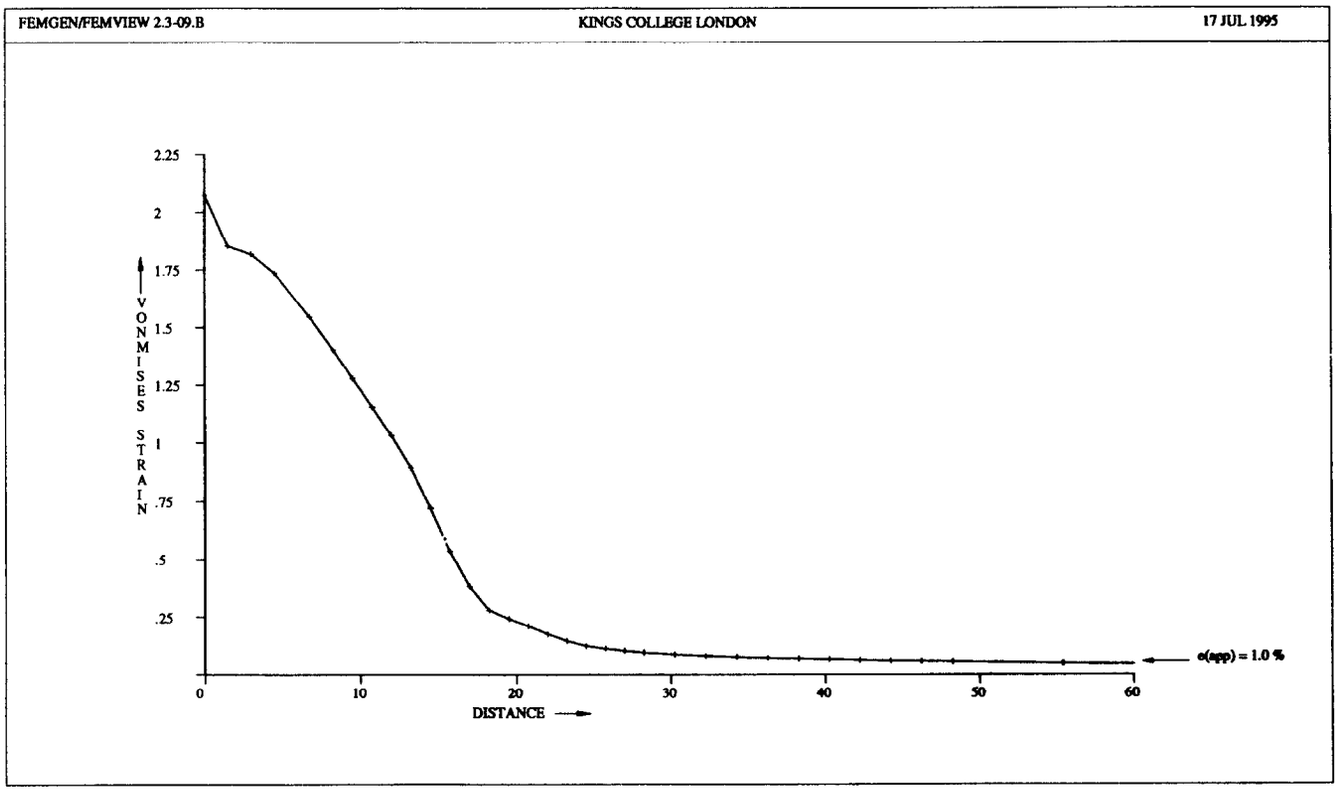

Figure 5 Simple fibre end model: interfacial von Mises strain distribution ($e_{app} = 1.0\%$)

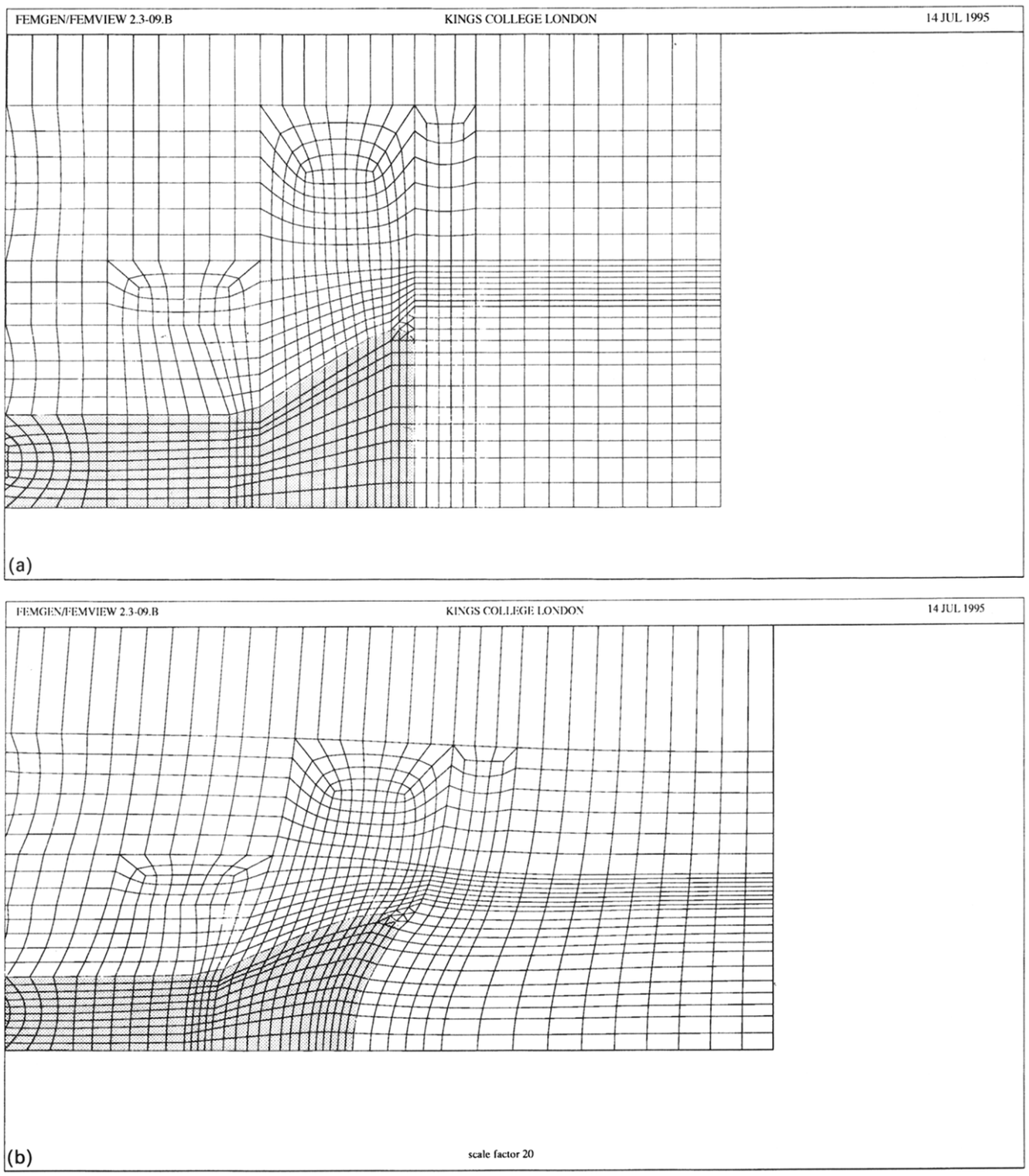

Figure 6 (a) 1-D FEFM: undeformed mesh; (b) 1-D FEFM: deformed mesh (scale factor 20) ($e_{app} = 0.5\%$); (c) 1-D FEFM: von Mises strain contour map ($e_{app} = 0.5\%$)

region of the fibre end are shown in *Figures 6a* and *b*. The fibre is shown shaded and all the nodal displacements have been magnified by a scale factor of 20. A contour map of von Mises strain (*Figure 6c*), exhibits a maximum at the fibre corner of 7%, for an e_{app} of 0.5% (with thermal pre-load). This is more clearly observed in the interfacial von Mises strain distributions along the fibre (*Figure 7a*). The areas of strain concentration are at the fibre corner and in the region of matrix adjacent to the fibre end face.

The importance of the thermal pre-load in reducing von Mises strain concentrations may be understood with reference to *Figure 7b*, where the interfacial shear strain distributions are presented (E12 being the in-plane shear strain). The thermal pre-load causes a shear strain of the

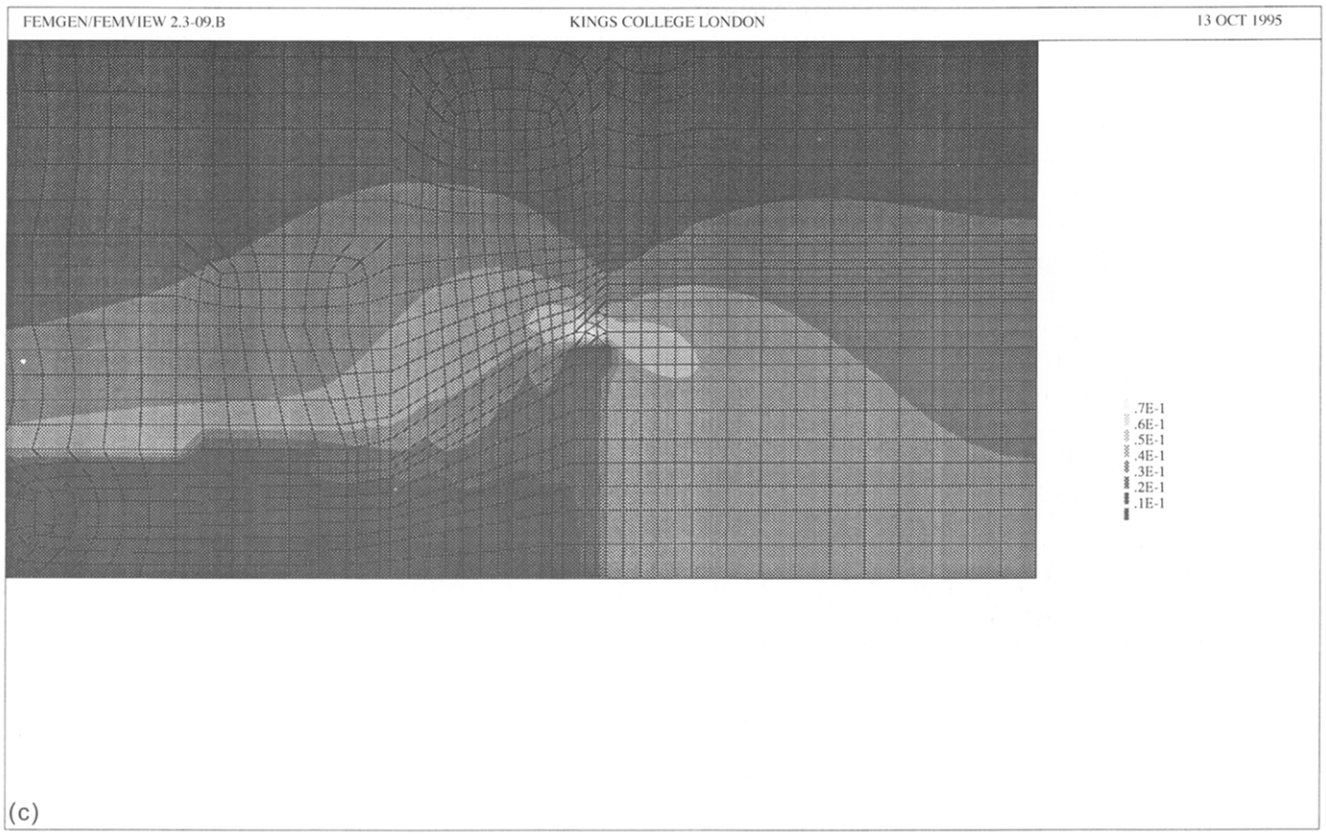

Figure 6 Continued

matrix at the interface (*Figure 7b*), in a manner opposite to the mesh deformations of *Figure 6b*. When subsequent applied strains are imposed on the thermally prestrained composite, shear strains opposite to the thermal shear strains are observed. Thus, a shear strain *reversal* has occurred. This effectively means that the thermal pre-load reduces the von Mises strain concentration, in any subsequent tensile loading, by an amount approximately equal to that generated by the thermal pre-load alone.

2-D FEFM

The von Mises strain contour map of the fibre end after the application of thermal pre-load and a subsequent applied strain of 0.5% (*Figure 8*), exhibits a similar pattern as the 1-D FEFM except that the von Mises strain concentration has reduced in value to 6%. There is also slightly more yielding in the fibrillated zone than before. The stress and strain fields are indicative of Mode α interfacial failure.

The FE axial stress distributions for e_{app} of 0.5 and 0.7% (*Figure 9a*), show very good correlation with the experimental data along the fibre length. For higher levels of e_{app} of 1.0 and 1.3% (*Figure 9b*), there is substantial discrepancy between the experimental data and the FE predicted profiles. The reason for this discrepancy is most probably due to the fact that a more complex mechanism of interfacial failure is occurring. This may be understood by considering the values of maximum von Mises strains at the fibre end. For the four levels of applied strain of 0.5, 0.7, 1.0 and 1.3%, the values of von Mises matrix strain maxima are 6, 10, 37 and 72% (as seen in *Figure 7a*), respectively. By substituting these values into criterion III, it may be seen that the last two values fail the criterion by a significant margin, thus indicating a fracture type of failure. The value of 10% is still double the quoted failure strain of 4.2%, but this is acceptable given that thin films of matrix tend to fracture at higher strains than the bulk matrix. This is attributed to the lower flaw density in thin films which otherwise act as failure-nucleation sites in the bulk matrix. A maximum acceptable value of matrix failure strain may be in the range 15–20%.

It may thus be postulated that at the higher levels of applied strain, a mode of interfacial failure other than pure Mode α is taking place. Thus it may be further said that an interfacial failure mode transition is occurring from pure Mode α to a mixture of Mode α with Mode β or γ.

CONCLUSIONS

Elasto-plastic FE modelling of the Kevlar fibrillated fibre end geometry has shown that Mode α interfacial failure exists on tensile loading of a composite specimen, at applied strains below 1.0%.

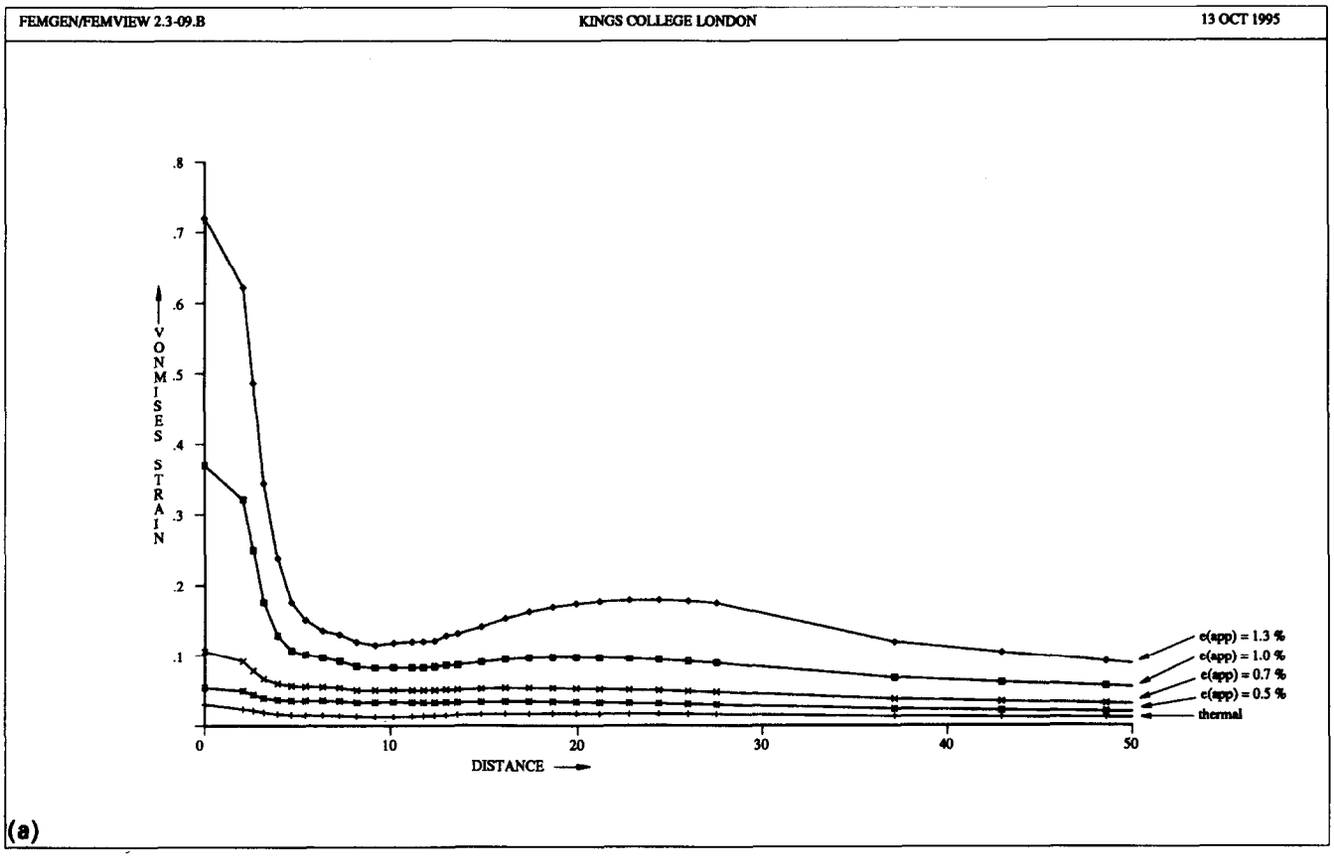

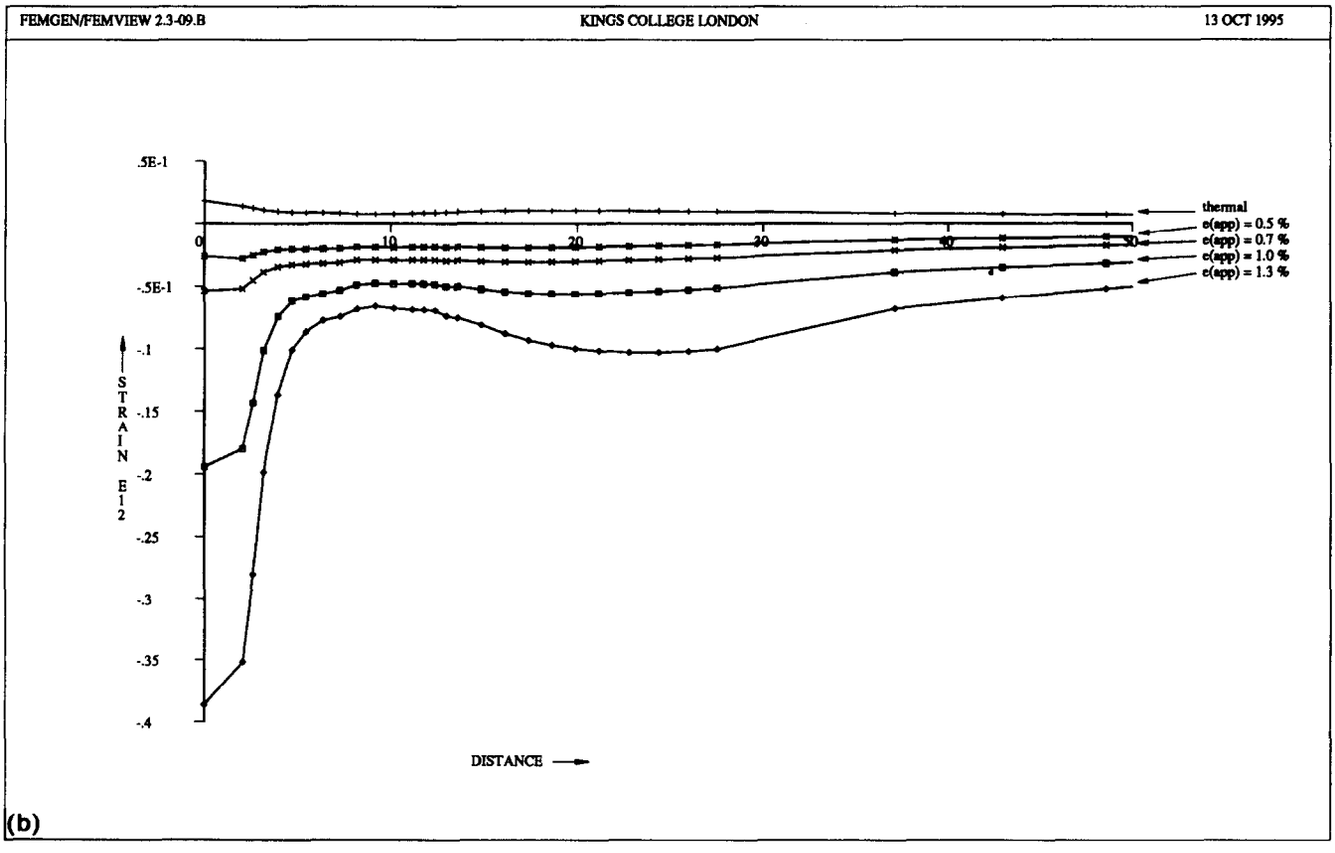

Figure 7 (a) 1-D FEFM: interfacial von Mises strain distributions; (b) 1-D FEFM: interfacial shear strain distributions

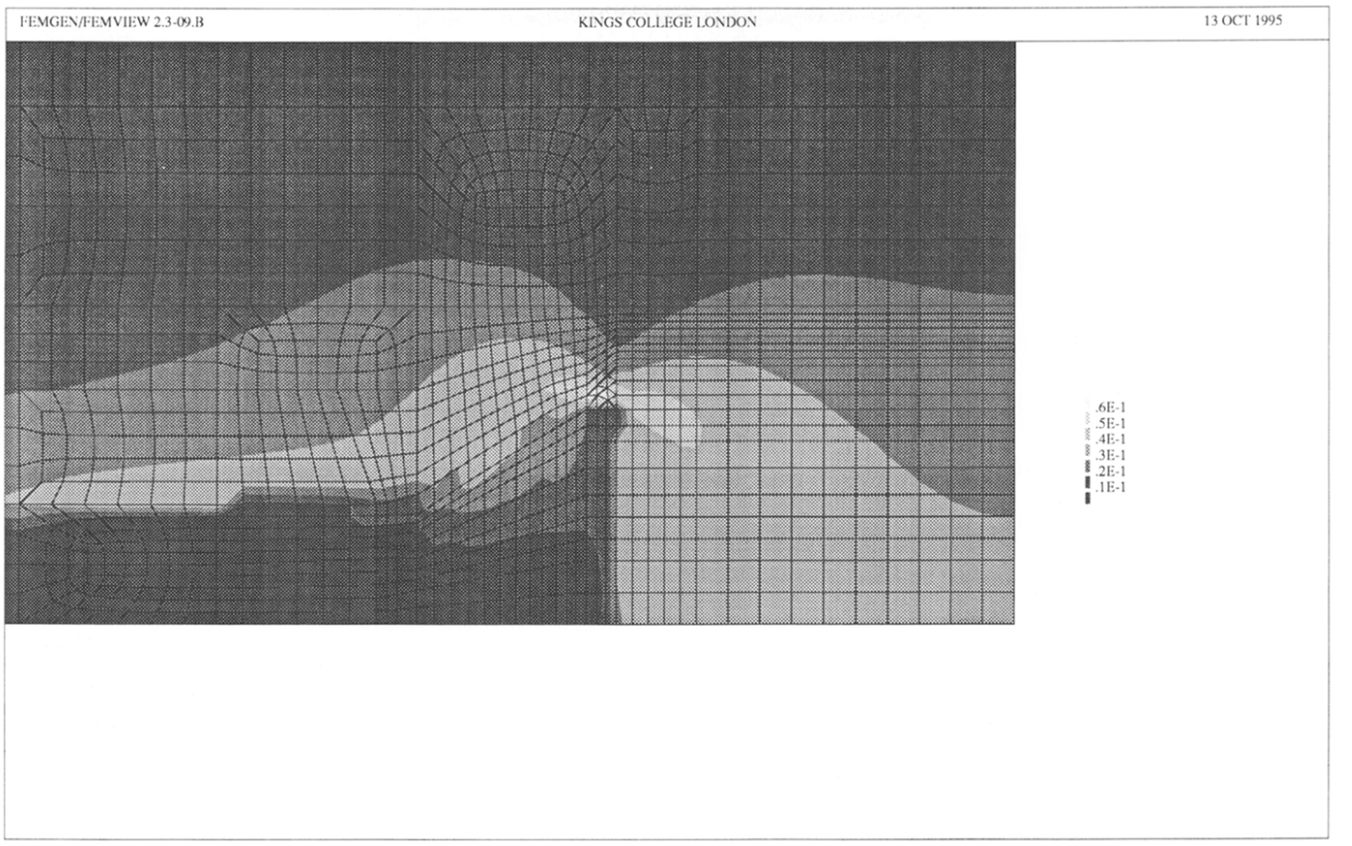

In order to correctly account for the fibrillated zone, use of a fibre end fibrillation model (FEFM) in its 1-D or 2-D forms has been made. This model accounts for the complex fibre–matrix interaction which occurs in short Kevlar fibres cut using ceramic scissors.

FE analyses have shown that the stress and strain fields in the matrix as predicted by the two FEFMs are similar. The precise fields may be important in trying to determine the exact location of fibre–matrix debonding, which will inevitably occur at higher levels of applied strain, since the 2-D FEFM predicts a slightly different stress and strain field from the 1-D FEFM. Since little difference has been found between the stress and strain fields of the 1-D and 2-D models, it may be concluded that the precise radial variation of elastic modulus is not a very important parameter. Hence the sensitivity of the overall solution with respect to discretisation of the fibrillated zone will be minimal.

The residual strains due to curing reduce the von Mises strain concentrations at the fibre–matrix interface once the composite is subsequently loaded in tension. This may have far-reaching implications for the design strength of composites, especially in low fibre volume-fraction composites where the thermal contraction of the matrix is significant.

At applied strains of 1.0% or higher, it is postulated that an interfacial failure mode transition occurs from pure Mode α to a mixture of Mode α with Mode β or γ.

A Mode α interfacial failure is consistent with the experimental data in the Kevlar–epoxy composite system, at low applied strains, whereas a Mode γ interfacial failure has been found to be consistent with experimental data in an unsized carbon–epoxy system[13,14]. The reason for the difference in interfacial failure mode has to do with the yield stress of the matrix *versus* the interfacial fracture toughness of the fibre–matrix system, on applied tensile loading of the composite. The competing failure mechanisms are dependent on fibre geometry and material property differentials between fibre and matrix. Carbon reinforced composites have a much higher elastic modulus differential than Kevlar composites, and more significantly, carbon fibres do not fibrillate on cutting. This suggests that Mode α is the dominant mode of interfacial failure for Kevlar 49 fibre reinforced composites at low levels of applied strain, whereas carbon fibre reinforced composites are more likely to undergo Mode β or γ interfacial failure.

ACKNOWLEDGEMENTS

Dr C. Vlattas is thanked for performing the experimental work described in this paper. One of us (RBN) wishes to thank Professor G. C. Papanicolaou for helpful discussions.

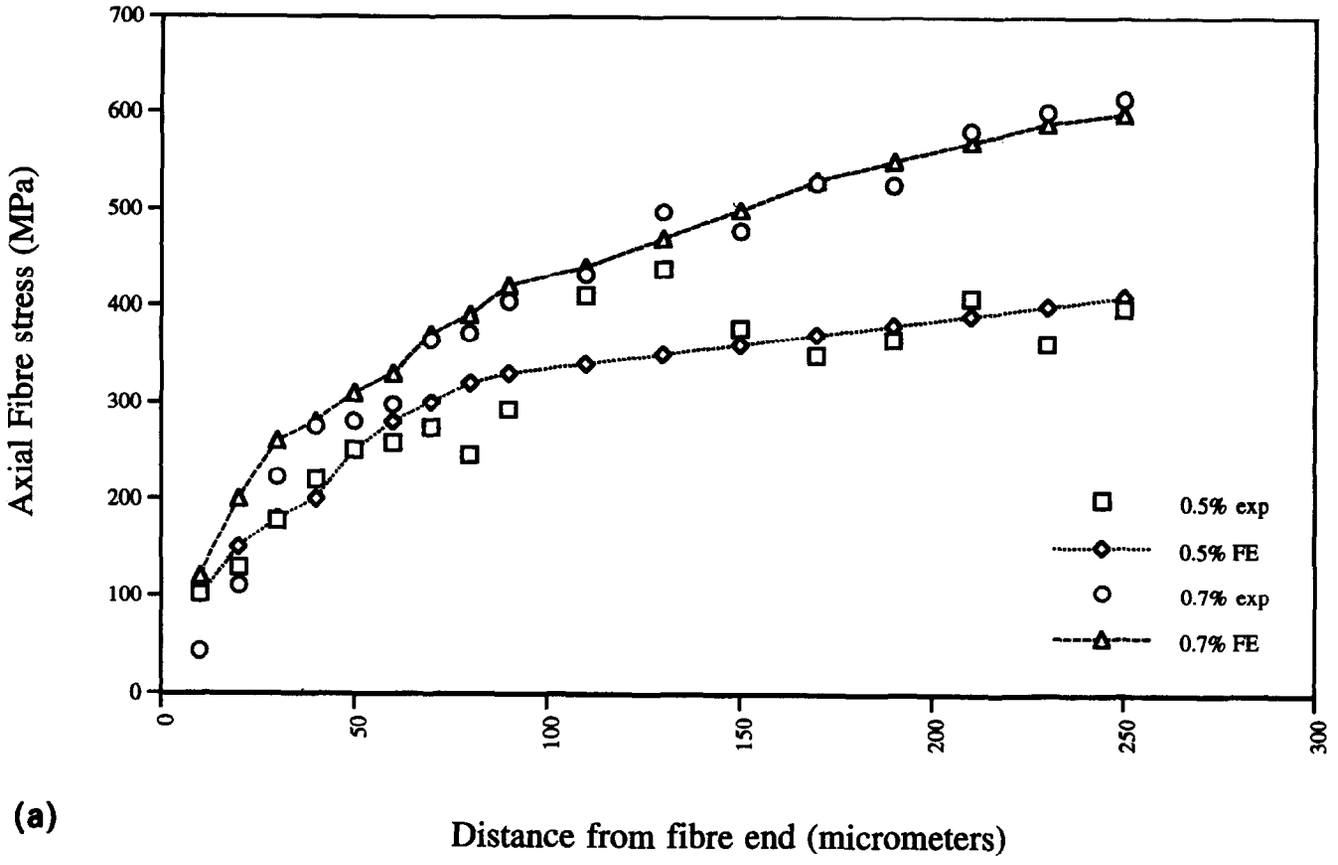

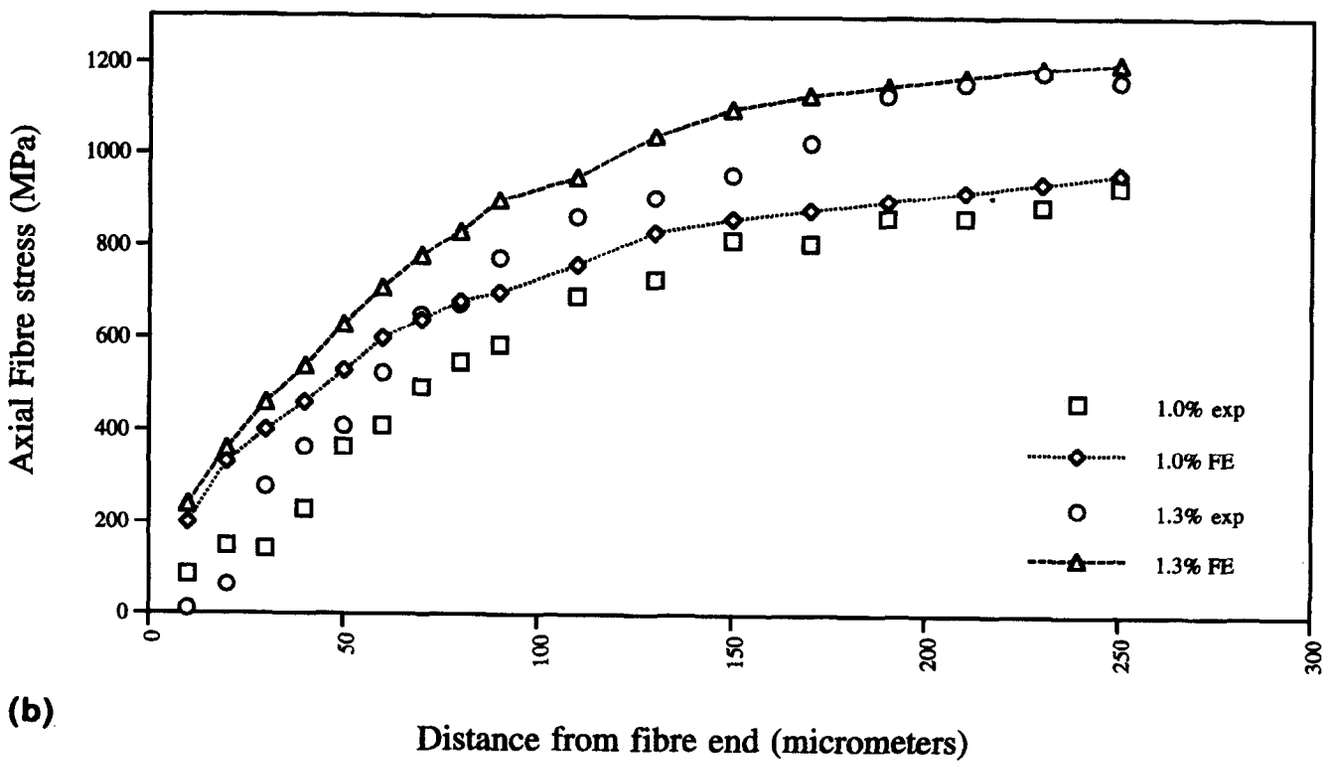

Figure 9 2-D FEFM: experimental and FE axial fibre stress distributions: (a) $e_{app} = 0.5, 0.7\%$; (b) $e_{app} = 1.0, 1.3\%$

REFERENCES

1 Cox, H.L. *Br. J. Appl. Phys.* 1952, **3**, 72
2 Vlattas, K. *PhD thesis*, Queen Mary & Westfield College, London, 1995
3 Melanitis, N., Galiotis, C., Tetlow, P.L. and Davies, C.K.L. *J. Compos. Mater.* 1992, **26**, 574
4 Guild, F.J., Vlattas, C. and Galiotis, C. *Compos. Sci. Technol.* 1994, **50**, 319
5 Galiotis, C. *Compos. Sci. Technol.* 1993, **48**, 15
6 Vlattas, C. and Galiotis, C. in 'Developments in the Science and Technology of Composite Materials', ECCM-5 (Eds A.R. Bunsell, J.F. Jamet and A. Massiah), European Association of Composite Materials, Bordeaux, 1992, p. 415
7 Galiotis, C. *Compos. Sci. Technol.* 1991, **42**, 125
8 Melanitis, N. and Galiotis, C. *Proc. R. Soc. London, Series A* 1993, **40**, 79
9 Melanitis, N., Galiotis, C., Tetlow P.L. and Davies, C.K.L. *J. Mater. Sci.* 1993, **28**, 1648
10 Sato, N., Kurauchi, T., Sato, S. and Kamigaito, O. *J. Compos. Mater.* 1988, **22**, 850
11 Jones, K.D. and DiBenedetto, 'Deformation and Fracture of Composites '95', The Institute of Materials, London, 1995, p. 86
12 Busschen, A.ten and Selvadurai, A.P.S. *J. Appl. Mech.* 1995, **62**, 87
13 Nath, R.B., Fenner, D.N. and Galiotis, C. *J. Mater. Sci.* 1995, submitted
14 Nath, R.B., Fenner, D.N. and Galiotis, C. 'Deformation and Fracture of Composites '95', The Institute of Materials, London, 1995, p. 606
15 Cook, R.D. 'Finite Element Modelling for Stress Analysis', Wiley, London, 1995
16 Shi, N., Wilner, B. and Arsenault, R.J. *Acta Metall. Mater.* 1992, **40**, 2841
17 Busschen, A.ten and Selvadurai, A.P.S. *J. Appl. Mech.* 1995, **62**, 98
18 Sun, C.T. and Wu, J.K. *J. Reinf. Plastics and Compos.* 1984, **3**, 130
19 Daoust, J., Vu-Khanh, T., Ahlstrom, C. and Gerard, J.F. *Compos. Sci. Technol.* 1993, **48**, 143
20 Nassehi, V., Dhillon, J. and Mascia, L. *Compos. Sci. Technol.* 1993, **47**, 349
21 Marotzke, C. *Compos. Sci. Technol.* 1994, **50**, 393
22 Termonia, Y. *J. Mater. Sci.* 1987, **22**, 504
23 Berthelot, J.-M., Cupcic, A. and Brou, K.A. *J. Compos. Mater.* 1993, **27**, 1391

APPENDIX

Fibre end fibrillation models (FEFM)

To take account of the material property variation in the z direction, we consider an infinitesimally thin elemental cylinder within the fibrillated zone (*Figure 2*), with a mean radius r_{cyl} and thickness dz. The cylinder is assumed to contain a mixture of fibre fully interspersed with the matrix, where v_f and v_m are the respective volume fractions. The volume of fibre in the cylinder is equal to the volume of the fibre in the unfibrillated fibre, radius r_f. Thus:

$$v_f = (A_f dz)/(A_{cyl} dz)$$

where A_{cyl} and A_f are the cross-sectional areas of the cylinder and unfibrillated fibre, respectively. The fibre is considered to be transversely isotropic and linear elastic, and the matrix to be isotropic and non-linear elasto-plastic. Following a *rule of mixtures* argument, the tensile moduli of the cylinder are a weighted average of those of the fibre and matrix, given by

$$E_{cyl}(\epsilon) = E_f \cdot v_f + E_m(\epsilon) \cdot (1 - v_f)$$

where E_{cyl} is the cylinder tensile modulus in a coordinate direction, E_f is the fibre tensile modulus in a coordinate direction, E_m is the matrix tensile modulus in a coordinate direction and ϵ is the given level of strain.

Substituting for v_f, we have:

$$E_{cyl}(\epsilon) = E_f \cdot \{A_f/A_{cyl}\} + E_m(\epsilon) \cdot (1 - \{A_f/A_{cyl}\})$$

which simplifies to yield:

$$E_{cyl}(\epsilon) = E_f \cdot \{r_f/r_{cyl}\}^2 + E_m(\epsilon) \cdot (1 - \{r_f/r_{cyl}\}^2)$$

Similarly, for the shear moduli, we have the corresponding expression:

$$G_{cycl}(\epsilon) = G_f \cdot \{r_f/r_{cyl}\}^2 + G_m(\epsilon) \cdot (1 - \{r_f/r_{cyl}\}^2)$$

where G_{cyl} is the cylinder shear modulus in a coordinate plane, G_f is the fibre shear modulus in a coordinate plane and G_m is the matrix shear modulus in a coordinate plane.

Since the second term in each equation is always much smaller than the first term, over the range of strain considered, we may neglect the non-linearity of the matrix stress–strain curve, without much error. This simplifies the equations to give:

$$E_{cyl} = E_f \cdot \{r_f/r_{cyl}\}^2 + E_m \cdot (1 - \{r_f/r_{cyl}\}^2)$$

$$G_{cyl} = G_f \cdot \{r_f/r_{cyl}\}^2 + G_m \cdot (1 - \{r_f/r_{cyl}\}^2) \qquad \text{(A1)}$$

Both equations define the variation for all the various elastic moduli, since the fibrillated zone is transversely isotropic due to the influence of the fibre. Hence, the elastic moduli of a given cylinder are solely functions of axial coordinate, z, along the fibrillated zone; as z decreases, r_{cyl} increases linearly. When $r_f = r_{cyl}$ the equations reduce to the desired result for the fibre elastic moduli.

In the 2-D FEFM, we consider that the material properties vary in both the axial and radial directions. It is probable that towards the axis of the fibrillated zone, penetration of the matrix becomes progressively more difficult. The extent of fibril dilution by the matrix will therefore be maximum at the periphery of any given cylinder, and minimum at the axis. Thus, the material in the peripheral region of the fibrillated zone will have lower elastic moduli than that nearer the axis. It is assumed that the variation of material properties is linear with radial axis coordinate, and also that the elastic moduli at the axis of the zone are three times their corresponding values at the periphery. The average value of the radially varying tensile elastic modulus of a given elemental cylinder, $E_{cr}(r)$, is equal to E_{cyl}. Hence, we have

$$E_{cr}(r) = ar + b$$

where a and b are coefficients determined by the

boundary conditions:

$$E_{cr}(0) = 1.5\,E_{cyl} \qquad E_{cr}(r_{cyl}) = 0.5\,E_{cyl}$$

Solving for a and b, we have for the tensile and shear moduli variations

$$E_{cr}(r) = E_{cyl}\{3/2 - r/r_{cyl}\}$$
$$G_{cr}(r) = G_{cyl}\{3/2 - r/r_{cyl}\} \qquad \text{(A2)}$$